Available online at www.sciencedirect.com
ScienceDirect
Polymer 48 (2007) 7393–7403
polymer
www.elsevier.com/locate/polymer

Radiation effects and re-crystallization mechanism of syndiotactic polystyrene with β′-crystalline form

Chi Wang*, Chien-Lin Huang, Yong-Wen Cheng, Yu-Chen Chen, Jasmine Shong

Department of Chemical Engineering, National Cheng Kung University, Tainan 701, Taiwan, ROC

Received 26 July 2007; received in revised form 7 September 2007; accepted 6 October 2007
Available online 14 October 2007

Abstract

The double melting behavior of syndiotactic polystyrene (sPS) with β′-form crystallites was systematically investigated by several analytical techniques, including differential scanning calorimetry (DSC), polarized light microscopy (PLM), transmission electron microscopy (TEM), as well as wide-angle and small-angle X-ray scattering (WAXD, SAXS). For preventing the possible chain re-organization during intermediate melting, a high-energy electron beam (e-beam) radiation was carried out on the melt-crystallized samples to chemically cross-link the amorphous chains between lamellar crystals. The WAXD intensity profiles of the irradiated sPS samples revealed that no crystal transformation took place, and the crystallinity fraction remained unchanged for a received dose up to 2.4 MGy. As the received dose was increased, however, the high melting temperature peak was gradually diminished and finally disappeared after 1.8 MGy e-beam radiation, suggesting that the double melting phenomenon was mainly attributed to the melting/re-crystallization/re-melting behavior. The re-crystallization mechanism of sPS samples was studied using DSC and PLM to reveal the effects of heating rate and annealing temperature on the Avrami exponent and re-crystallization rate constant. In addition, the lamellar morphologies of the re-crystallized samples were also investigated by means of SAXS and TEM. With increasing heating rate or annealing temperature, the derived Avrami exponent was slightly decreased from 1.4 to 1.1; in comparison, the re-crystallization rate showed a shallow maximum at a rate of 10 °C/min, but it became evidently reduced at high annealing temperatures. Based on the morphological observations, we proposed that the re-crystallization of β′-form sPS crystals involved with the presence of broad lamellar thickness distribution as well as abundant irregular loose folding chains on the lamellar surfaces, which became tightened and crystallized into the un-melted lamellae when the neighboring thinner lamellae trapped in-between were melted. Thus, the high melting temperature is dependent on the average thickness of lamellae consisting of the un-melted lamellae developed initially and thickened ones associated with re-crystallization.

Keywords: Double melting; Syndiotactic polystyrene; Re-crystallization

1. Introduction

Differential scanning calorimetry (DSC) heating traces are frequently applied to a crystallized polymer sample to determine its melting point and heat of fusion; the former gives the perfection and/or the thickness of the lamellae, while the latter provides the relative amount of chains which constitute the ordered region. It is of great interest to note that the DSC heating traces of certain polymers, such as poly(ethylene terephthalate) [1,2], poly(ether ether ketone) [3–6], and isotactic PS [7], which have been isothermally crystallized, show multi-melting endotherms.

The presence of multi-melting endotherms may be attributed either to different crystal structures (polymorphism) [8,9], different lamellar thicknesses and/or perfection [4,10], or crystal re-organization during heating trace [1,5,11,12]. Specifically, the dual lamellar thickness model includes two branches: the lamellar insertion model and the dual lamellar stack model [13,14]. In support of the two-morphology models, some researchers have found that the high-temperature endotherm is developed prior to the low-temperature

* Corresponding author. Tel.: +886 6 2757575x62645; fax: +886 6 2344496.
E-mail address: chiwang@mail.ncku.edu.tw (C. Wang).

0032-3861/$ - see front matter © 2007 Elsevier Ltd. All rights reserved.
doi:10.1016/j.polymer.2007.10.012

one, and two distinct lamellar populations are observed using transmission electron microscopy (TEM) [4,6]. On the other hand, a crystallization exotherm between the two melting peaks is often observed when the samples are crystallized at a high undercooling. This suggests the validity of the re-crystallization model as well. According to the melting/re-crystallization model, the low endotherm presents the melting of the initially crystallized lamellae; during continuous annealing, part of the melted lamellae will re-crystallize into thicker (more perfect) lamellar crystals, which melt at a higher temperature. As a complimentary technique, small-angle X-ray scattering (SAXS) is also frequently applied to monitor the variation of morphological lengths during the double melting process. Depending on the systems, the SAXS results supported both the dual lamellar thickness model [15] and the re-crystallization model [11]. A recent review of the multi-melting behavior of semi-stiff polymers was given by Verma and Hsiao [13].

Depending on the crystallization condition, the syndiotactic polystyrene (sPS) demonstrates the ability to form different crystal structures due to its polymorphic nature. When crystallized from the melt, sPS develops either hexagonal (α form) or orthorhombic (β form) modifications with a zig–zag chain configuration [16–19]. Previous results showed that β-form modification is thermodynamically favored, whereas α-form modification is preferentially induced by a kinetically-controlled process or a memory effect [16]. Further classification leads to two limiting order structures, denoted by α'-, β'- and α''-, β''-form, respectively, for the disordered and ordered structures associated with the packing of molecules within the crystals [16,19]. In general, the DSC heating traces on the β'-form sPS melt-crystallized at low crystallization temperatures (T_c) exhibit two distinct melting endotherms, whereas only one melting peak is observed for samples that were melt-crystallized at high T_c [20–23]. In contrast, a single melting peak was essentially observed for the sample with β'' modification [24]. In this study, we focused on the sPS samples with β'-form crystals. Guerra et al. [16,24] have demonstrated that no crystal transformation (either $\beta' \rightarrow \alpha$ or $\beta' \rightarrow \beta''$) would take place, but morphological variation should be more relevant to account for the double melting behavior of the β'-form sPS. Sun and Woo [25] reported a more complicated melting behavior of sPS samples: three melting peaks were observed for β'-form sPS melt-crystallized at a lower temperature (e.g. $T_c = 230$ °C) or heating with a lower heating rate (e.g. 5 °C/min for sPS crystallized at $T_c = 240$ °C). Although extensive studies on the multiple melting behavior of sPS had been conducted, the assignment of individual melting peak and the deduction were primarily based on the results obtained from DSC, wide-angle X-ray diffraction (WAXD), and scanning electron microscopy (SEM) [20–25], which provided indirect or relatively rough information on individual lamellae during the melting process. To our knowledge, there has been no detailed study yet exploring morphological changes during the melting of sPS lamellae.

In this article, we attempted to revisit the double melting behavior of β'-form sPS using TEM and SAXS to obtain a fine observation of lamellar morphologies. In addition to DSC measurements, the changes in spherulitic morphologies and re-crystallization kinetics associated with sPS melting were also studied by a polarized light microscope (PLM). To elucidate the origin of the double melting behavior, electron beams (e-beams) were first applied on the melt-crystallized samples for inducing the cross-linking network structure of the amorphous chains between lamellae to prohibit the possible re-organization during melting. With increasing radiation dose, the higher melting peak was gradually suppressed and disappeared at a dose higher than 1.8 MGy. In comparison, the lower melting peak was stable up to 0.8 MGy dose. Based on these findings, the bimodal lamellar structures were excluded for accounting for the double melting phenomena, and the lower melting temperature was indicative of the melting of the original lamellae presented in the crystallized samples. The re-crystallization mechanism and morphologies developed after partial melting were also studied using DSC, PLM, TEM, WAXD, and SAXS. The kinetics of the re-crystallization process was analyzed via Avarmi equation. The effects of the heating rate and annealing temperatures on the re-crystallization kinetics were investigated, and the plausible re-crystallization mechanism was provided as well.

2. Experimental

sPS pellets with a weight average molecular weight of 200 kg/mol were supplied by Dow Chemical Co. To prepare sPS samples in β' form, the pellets were hot-pressed at 290 °C and 0.6 MPa for 10 min, followed by ambient cooling at ambient pressure. sPS discs (a diameter of 17 and 1.2 mm thick) were irradiated in air atmosphere using an electron beam accelerator. The electron energy was 1.8 MeV with a beam current of 6.4 mA. A conveyor system was used to transport the sPS discs with a speed of 10 m/min to receive the radiation step-by-step until the desired dose was built up. The samples were irradiated to total doses ranging from 0.1 to 2.4 MGy for further studies.

2.1. DSC measurements

The melting behavior and crystallization of the irradiated sPS samples were investigated using a Perkin–Elmer DSC7. Prior to measurements, indium and zinc standards were used to calibrate the enthalpies of fusion and melting temperatures. The melting enthalpy and temperature of the sPS samples were measured at a heating rate (R) of 10 °C/min (unless otherwise specified) under nitrogen atmosphere to diminish oxidation. The melting temperature was reported at the peak of the melting endotherm, and the area of endotherm gave the melting enthalpy, ΔH_m.

To study the re-crystallization kinetics, the temperature sequence was arranged as follows: the sample was melted at 300 °C for 10 min and cooled to 240 °C for isothermal crystallization for 4 min. Then the sample was heated at a rate of 10 °C/min to the selected annealing temperatures ($T_a = 251$, 261, 263, 265, 267, and 269 °C) for 12 min to reveal the

re-crystallization kinetics. The effect of heating rate on the re-crystallization kinetics was also investigated by applying various R to heat the 240 °C-crystallized samples to $T_a = 267$ °C.

2.2. PLM light intensity measurements

A polarized light microscope (PLM, Leica DMLP) equipped with a hot stage (THMS600, Linkam) and an AP1 camera (Apogee Instruments Inc.) was used to monitor the variation of depolarized light intensity during isothermal crystallization and the melting of sPS as well [26]. Prior to the measurements, the hot stage was calibrated with benzoic acid and tin. The samples were first maintained at 300 °C for 10 min and then quickly cooled to the desired temperature for crystallization. After crystallization, subsequent melting was performed at a heating rate of 10 °C/min. The camera possesses a 16-bit dynamic range Charge Coupled Detector (CCD) with a resolution of 768 × 512 pixels. Automatic storage of the images was conducted by the recording system at a time interval of 2.8 s, leading the temperature resolution to be 0.24 °C for accuracy. Under crosspolars, the high-performance CCD imaging system will give the intensity change of the depolarized light during crystallization and melting process.

2.3. WAXD measurements

WAXD measurements were frequently carried out to ensure the neat β′ crystalline form of the as-prepared samples. A rotating-anode X-ray generator (Philips, PW1710) with mono-chromatized Cu Kα X-ray beam was used. The generator was operated at 40 kV and 100 mA, and the data were collected from 5 to 30° in 2θ in steps of 0.02° at a scanning rate of 4°/min.

2.4. SAXS measurements

SAXS studies were performed at room temperature using a 18 kW rotating-anode X-ray generator (Cu target, Rigaku) operated at 40 kV and 200 mA. A set of three pinhole collimators was used. A two-dimensional position-sensitive detector (ORDELA Model 2201X, Oak Ridge Detector Laboratory Inc.) with 256 × 256 channels was used, and the sample-to-detector distance was set at 4000 mm. The area scattering intensities were averaged radially to obtain the one-dimensional intensity profile for further analyses. The scattering vector q (=4πsin θ/λ, where 2θ is the scattering angle and λ is the wavelength of X-ray) ranges from 0.11 to 3.0 nm^{-1}. Details of SAXS setup was described elsewhere [27]. For materials with diffuse phase boundaries, the Porod law predicts the scattered intensity at large angles, as follows [28]:

$$\lim_{q\to\infty}\left[K_p - \left(I_{raw} - I_{fl}\right)q^4\exp\left(\sigma^2q^2\right)\right] = 0 \quad (1)$$

where I_{raw} is the raw intensity, I_{fl} is the intensity arising from thermal density fluctuations, K_p is the Porod constant, and σ is the interfacial thickness between the crystalline and amorphous regions. A numerical simulation was carried out to obtain the optimal parameters (I_{fl}, K_p and σ). Then, corrected intensities, $I_{cor} = (I_{raw} - I_{fl})\exp(\sigma^2q^2)$, were used for further analyses.

2.5. TEM observations

The ultrathin films, ca. 50 nm thick, to be observed by TEM were prepared by sectioning the bulk samples at room temperature using an Ultracut UCT (Leica) microtome. The staining of the ultrathin films was subsequently carried out with ruthenium tetraoxide (RuO_4) vapors at room temperature. The TEM micrographs shown in this work were obtained by using JEM-2000FX (Jeol) operated at 80 kV.

3. Results and discussion

3.1. Radiation effects on the melting and subsequent dynamic crystallization

Prior to e-beam radiation, the samples were isothermally crystallized at 250 °C for 2 h for complete crystallization, followed by the 10 °C/min cooling to ambient temperature. The formation of β′-form sPS crystals in these samples was verified by their WAXD intensity profiles. After receiving various doses (0–2.4 MGy), the irradiated samples still preserved the β′-form crystals according to their WAXD intensity profiles as shown in Fig. 1 along with the indexed planes for each diffraction peaks [16]. The intensity profile of the completely amorphous sample is also given in Fig. 1 as dashed lines in an attempt to determine the crystallinity fraction (ϕ^{WAXD}). After resolving the intensity profiles associated with the amorphous halo and crystalline regions, respectively, ϕ^{WAXD} was estimated from the ratio of integrated intensities from all the

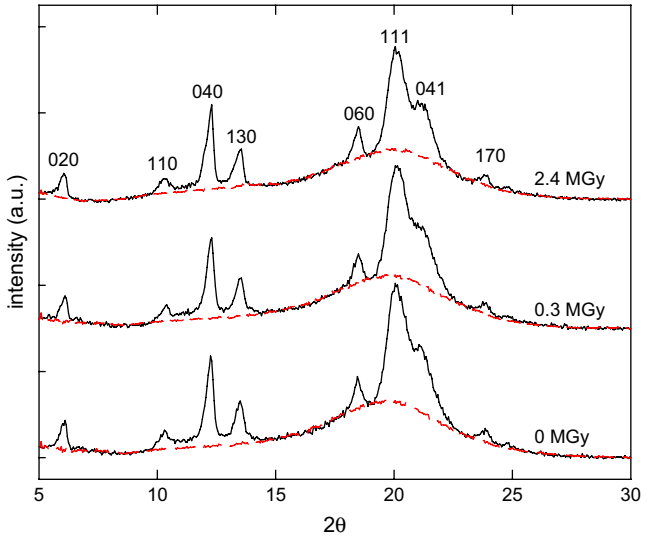

Fig. 1. WAXD intensity profiles of irradiated sPS samples with varying e-beam doses. The dashed line is the contribution of amorphous phase. The diffraction planes are indexed for the β′-form crystal modification. Prior to e-beam radiation, the sample is isothermally crystallized at 250 °C for 2 h.

diffraction peaks to the total intensity curve [27]. For the irradiated samples, no crystal transformation was observed, and ϕ^{WAXD} was unchanged (~0.38) regardless of the radiation dose, implying the radiation stability of the β′-form lamellae up to a received dose of 2.4 MGy. Nevertheless, the exposure of the crystallized sPS samples to high-energy radiation usually results in two typical chemical changes taking place in the inter-lamellar amorphous region, namely, main-chain scission and cross-linking [29,30]. The former is favored by a low radiation dose, while the latter takes place under excessive radiation. Indeed, our irradiated samples showed a color change from white to brown at a received dose of 0.8 MGy, and it became more prominent while the dose is increased mainly due to the formation of double bonds and oxidation. For the amorphous atactic PS (aPS), previous studies have demonstrated the possession of a high degree of resistance to γ-radiation in air due to the protective influence of the benzene ring, and that a radiation dose of 1.25 MGy was required to form a permanent cross-linking network [31].

Fig. 2 shows DSC melting traces of the irradiated sPS samples from ambient temperature to 300 °C at a heating rate of 10 °C/min. After exposure at 300 °C for 10 min, the subsequent cooling thermograms are displayed in Fig. 3 for revealing the cross-linking effects on the dynamic crystallization. In the absence of e-beam radiation, the crystallized sPS showed two melting peaks (Fig. 2), with the low and high peak temperatures referred to as T_{ml} and T_{mh} at 264.1 and 270.8 °C, respectively. As the radiation dose was increased, the high melting peak was gradually suppressed, shifted to a lower temperature, and finally became a barely discernible shoulder at a received dose of 1.2 MGy, accompanied by a T_{ml} reduction to 263.4 °C. Eventually, a single melting peak centered at 262.4 °C was observed for the samples undertaken at 1.8 MGy e-beam radiation. It is evident that e-beam radiation on the melt-crystallized sample has effectively induced the cross-linking reaction of the amorphous chains between

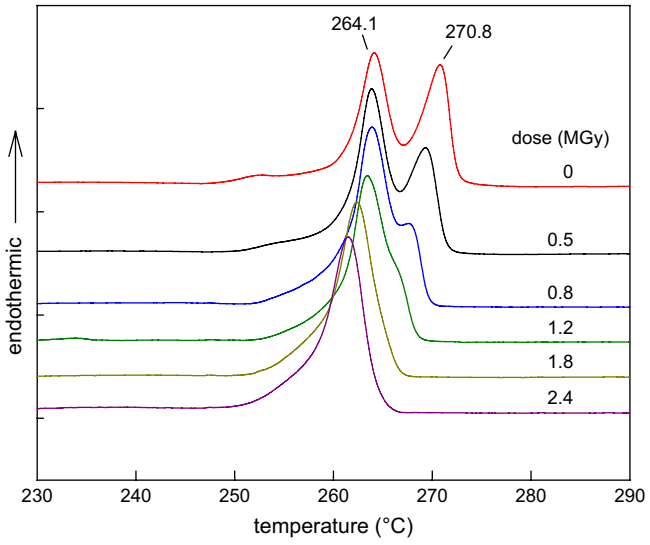

Fig. 2. Melting behavior of irradiated sPS samples with varying e-beam doses; heating rate: 10 °C/min.

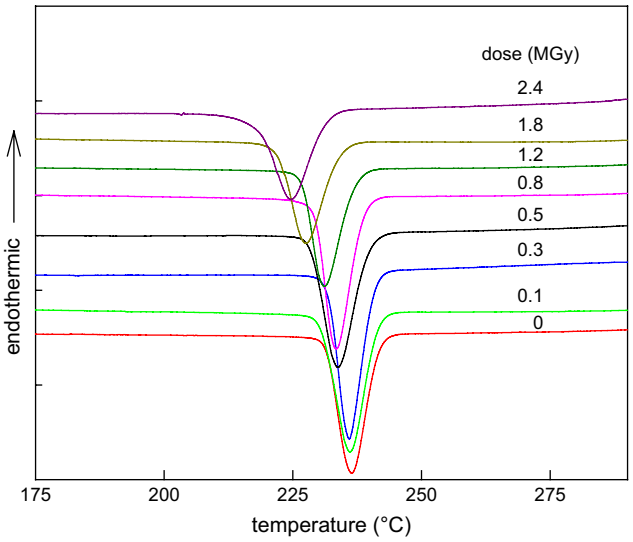

Fig. 3. Cooling scans of irradiated sPS samples with varying e-beam doses; cooling rate: 10 °C/min. Prior to the cooling scan, the sample is held at 300 °C for 10 min.

lamellar crystallites, leading to the hindrance of the plausible re-organization after the intermediate crystal melting. According to Fig. 2, a received dose higher than 1.2 MGy is sufficient to develop an effective chain network between crystalline lamellae for preventing re-crystallization. The radiation dose dependence of T_{ml} implies that the thickness of the lamellae plausibly remains unchanged for a dose lower than 0.8 MGy, but higher doses lead to a slight reduction of the lamellar thickness and/or destruction of crystal structure. Moreover, the cross-linking reaction gives rise to the branching and/or network microstructure of sPS chains which further retard the dynamic crystallization as shown in Fig. 3. Moreover, the crystallization peak temperature is decreased with an increase in radiation dose from 236.5 °C for the pristine samples to 224.7 °C for those receiving 2.4 MGy doses. Fig. 4 shows the radiation dose effects on melting enthalpy (ΔH_m) obtained by the heating scans (Fig. 2), the crystallization enthalpy

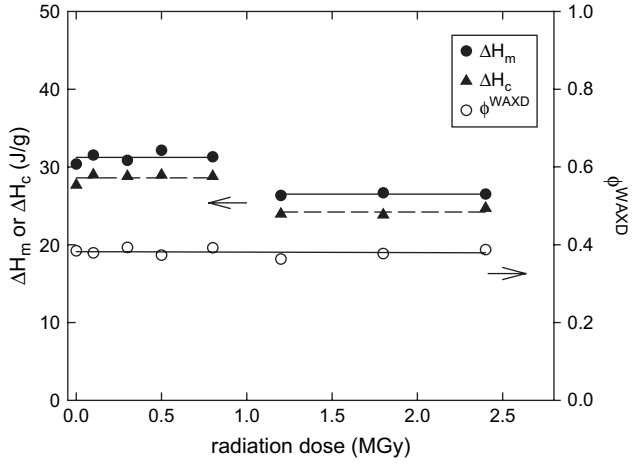

Fig. 4. Radiation dose dependence of ϕ^{WAXD} (open circles), ΔH_m (filled circles), and ΔH_c (filled triangles) for the crystallized sPS samples.

(ΔH_c) obtained by the cooling scans (Fig. 3), and the crystallinity fraction (ϕ^{WAXD}). ΔH_m was found to be slightly larger than ΔH_c regardless of the radiation dose. It is of interest to note that ΔH_m of the irradiated samples remained constant at 31.2 ± 0.7 J/g until a received dose of 1.2 MGy, where a transition was noticed by a dropping of ΔH_m to 26.5 ± 0.2 J/g. A further increase in the radiation dose up to 2.4 MGy did not affect the melting enthalpy. This trend suggested that the re-crystallization of the irradiated samples during crystal melting was completely suppressed for a received dose higher than 0.8 MGy. For the measured ΔH_c, a similar dependence of radiation dose was also observed with a corresponding ΔH_c drop from 28.6 ± 0.7 J/g at a low level to 24.2 ± 0.5 J/g at a high level of radiation.

However, the melting enthalpy for the 100% pure β′-form sPS crystals (ΔH_f^o) is still uncertain due to their polymorphism and complex melting behavior as shown in Fig. 2. At present, two distinct values, 52 J/g [32] and 82 J/g [33], have been reported in the literature without providing a detailed crystal modification assignment. Based on Fig. 4, our study's radiation results seem to provide a feasible route for the estimation of the ΔH_f^o value by assuming that the crystallinity fractions determined from WAXD and DSC are identical. To exclude the re-crystallization effect on the measured ΔH_m, only the ΔH_m results measured from the highly irradiated samples are considered for calculations. In this manner, the derived ΔH_f^o value is ca. 69.0 J/g for the pure β′-form crystals.

3.2. Radiation effects on isothermal crystallization and subsequent melting

In addition to the non-isothermal crystallization (Fig. 3), the isothermal crystallization of the irradiated samples was also conducted at 250 °C after exposure at 300 °C for 10 min. The heat release associated with crystallization was recorded, and the kinetics was analyzed by means of the Avrami equation to derive the overall crystallization rate (k), and Avrami exponent (n). As shown in Table 1, with an increase in the radiation dose, the peak time for the crystallization exotherm (t_{peak}) is larger, but the crystallization rate is smaller, both indicating the retardation of sPS crystallization. In addition, the Avrami exponent is gradually reduced from a value of 2.60 for the un-irradiated sample to 1.86 for those under high-level e-beam radiation, indicating the difference in the nucleation and growth mechanisms induced by the radiation. After the 250 °C isothermal crystallization, subsequent melting traces were also performed, and melting curves similar to those displayed in Fig. 2 were obtained. That is, double melting was still observed for a received dose lower than 0.8 MGy, but the high melting peak became less predominant in contrast with the "crystallized-irradiated" samples shown in Fig. 2.

Table 1
Effects of radiation dose on the Avrami exponent (n), overall crystallization rate (k), and crystallization peak time (t_{peak}) of irradiated sPS samples subjected to isothermal crystallization at 250 °C

Dose (MGy)	n	$k \times 10^3$ (min^{-1})	t_{peak} (min)
0	2.60	27	4.10
0.3	2.40	17	4.32
0.5	2.37	23	5.14
0.8	2.32	14	6.10
1.2	2.21	8.8	8.29
2.4	1.86	2.5	31.84

3.3. Re-crystallization kinetics studied by DSC

When the crystallization of the sPS samples took place at a lower T_c (such as 240 °C), the re-crystallization behavior during subsequent heating trace would become more significant as evidenced by the enhancement of the high melting peak. For revealing the re-crystallization kinetics more efficiently, therefore, the samples were herein melt-crystallized at 240 °C and then were heated to the intermediate temperatures to study the releasing enthalpy involved. The annealing of sPS at an intermediate temperature between T_{ml} and T_{mh} is an appropriate approach to reveal any thermal events involved during DSC heating trace [34]. For sPS melt-crystallized at 240 °C for 4 min, the values of T_{ml} and T_{mh} are 260.5 and 270.5 °C, respectively, at $R = 10$ °C/min. In comparison with the samples crystallized at 250 °C (Fig. 2), a lower T_{ml} is obtained but the T_{mh} is unchanged, giving a wider range of annealing temperature (T_a) available for re-crystallization investigations. Fig. 5 shows the effect of T_a on the samples which have been crystallized at 240 °C for 4 min and then were heated at 10 °C/min to the desired T_a. Since no crystal melting takes place at $T_a = 251$ °C, a flat baseline is expected. On the other hand, a crystallization exotherm is evident at $T_a = 261$ °C where there was partial melting of the low-temperature endotherm. As T_a is increased, the enthalpy (ΔH_{rc}) associated with the re-crystallization of the melted lamellae is increased (Table 2) and reaches a maximum at $T_a = 265$ °C, where the complete melting of the low-temperature endotherm takes place. A further increase of T_a leads to the reduction of re-crystallization extent (ΔH_{rc}). At an annealing temperature of 269 °C, there is no detectable exotherm, suggesting the inabilities of the melted lamellae to undergo re-crystallization at such a high temperature. Based on the Avrami equation, the exotherm associated with the re-crystallization was further analyzed to deduce the corresponding Avrami exponent and the rate of re-crystallization (k_{rc}). The derived values of n and k_{rc} are given in Table 2. It is of interest to note that k_{rc} is decreased with increasing T_a. This suggests that the transformation rate of the melted lamellae to the re-crystallized ones is reduced at a high T_a although the total amount of melted lamellae undergoing re-organization is higher. Moreover, one-dimensional crystal growth is expected since the derived n value is close to unity.

At a given T_a of 267 °C, Fig. 6 shows the annealing curves by applying various heating rates (R) on the sample, which has been melt-crystallized at 240 °C for 4 min. When a small R is applied, the melted crystals have been already re-crystallized during heating prior to reaching T_a, leading to a small ΔH_{rc} detected at 267 °C. When a too high heating rate is applied,

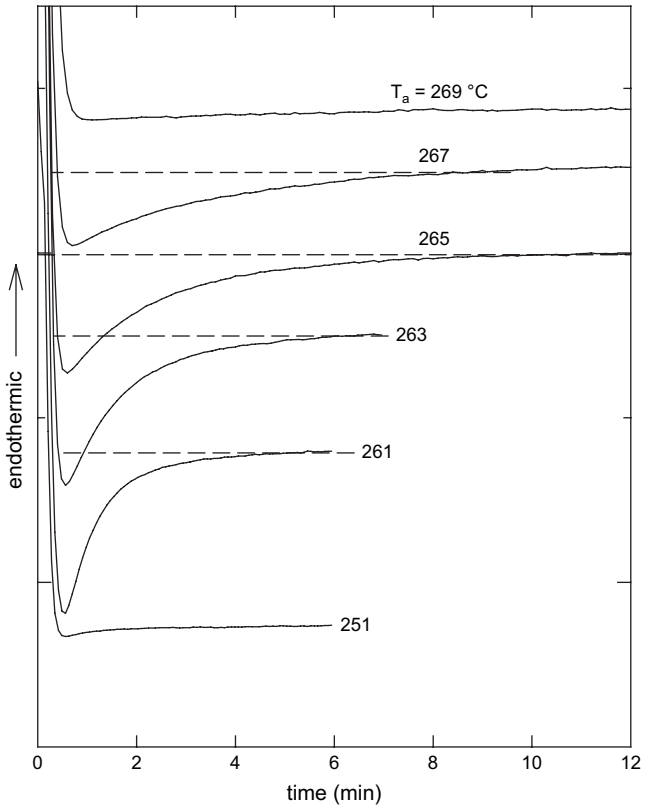

Fig. 5. Effects of annealing temperature, T_a, on the re-crystallization curves of sPS samples. sPS sample has been melt-crystallized at 240 °C for 4 min first, followed by a constant heating rate of 10 °C/min to various T_a for isothermal re-crystallization.

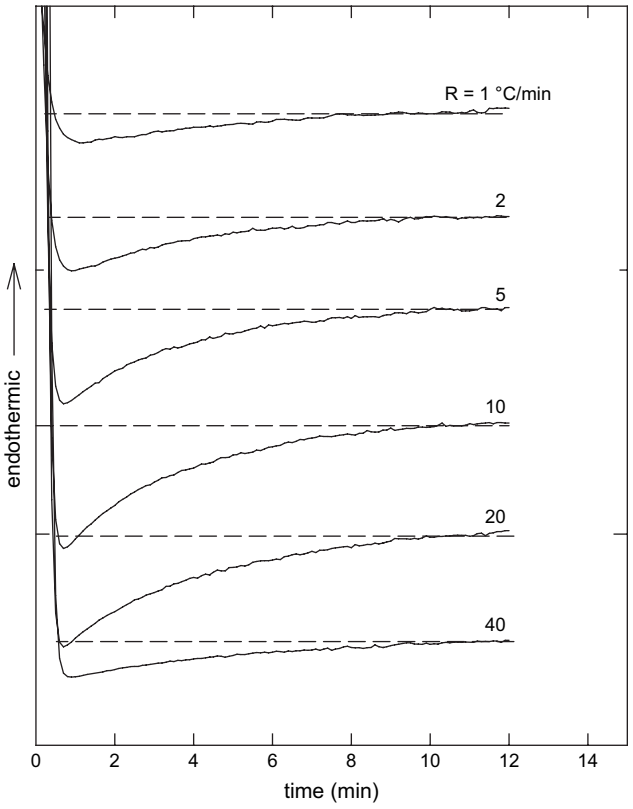

Fig. 6. Effects of heating rate, R, on the re-crystallization curves of sPS samples annealing at 267 °C. sPS sample has been melt-crystallized at 240 °C for 4 min first, followed by a subsequent heating to 267 °C for re-crystallization.

on the other hand, superheating effect inevitably takes place, and a small value of ΔH_{rc} is induced. Similar effects may also account for the presence of a shallow maximum of k_{rc} at 10 °C/min as shown in Table 3, where heating rate effects on the corresponding values of n, k_{rc}, and ΔH_{rc} are tabulated. The Avrami exponent is found to gradually decrease from 1.36 to 1.13 as the heating rate is increased from 1 to 40 °C/min. These values of n also suggest that one-dimensional crystal growth is involved in the re-crystallization process.

3.4. Re-crystallization kinetics studied by PLM

Using PLM coupled with a device for measuring transmitted light intensity, the isothermal crystallization kinetics and the subsequent melting behavior were feasibly analyzed [26]. This is based on the fact that the crystals developed in the spherulites are able to rotate the light passing through the polarizer to a certain level due to the optical anisotropic nature. This then facilitates a portion of transmitted light to be parallel to the analyzer which can be measured by the CCD camera. In the absence of existing crystals, on the other hand, no transmitted light can pass the analyzer and be detected by the CCD camera. Thus, the degree of crystallinity developed (or remained) within the spherulites is considered to be proportional to the intensity of the transmitted light measured [26,35]. Under crosspolar configuration, the plot of measured light intensities versus elapsed time is shown in Fig. 7; three sequences are involved, namely, *Stage I* (0–7.5 min) for isothermal crystallization at 250 °C and *Stage II* (7.5–9.3 min) for subsequent heating directly from 250 to 268 °C, followed by an isothermal annealing process at 268 °C for

Table 2
Effects of annealing temperatures (T_a) on the re-crystallization kinetics of sPS samples

T_a (°C)	n	k_{rc} (min^{-1})	ΔH_{rc} (J/g)
261	1.36	1.522	8.44
263	1.28	0.787	9.54
265	1.15	0.463	10.37
267	1.17	0.333	9.01

sPS sample has been melt-crystallized at 240 °C for 4 min first, followed by a subsequent heating at a rate of 10 °C/min to T_a for annealing.

Table 3
Effects of heating rates (R) on the re-crystallization kinetics of sPS samples annealed at 267 °C

R (°C/min)	n	k_{rc} (min^{-1})	ΔH_{rc} (J/g)
1	1.36	0.181	3.86
2	1.33	0.278	4.43
5	1.20	0.313	7.12
10	1.17	0.333	9.01
20	1.13	0.292	8.97
40	1.13	0.232	3.13

sPS sample has been melt-crystallized at 240 °C for 4 min first, followed by a subsequent heating at a rate of R to 267 °C for annealing.

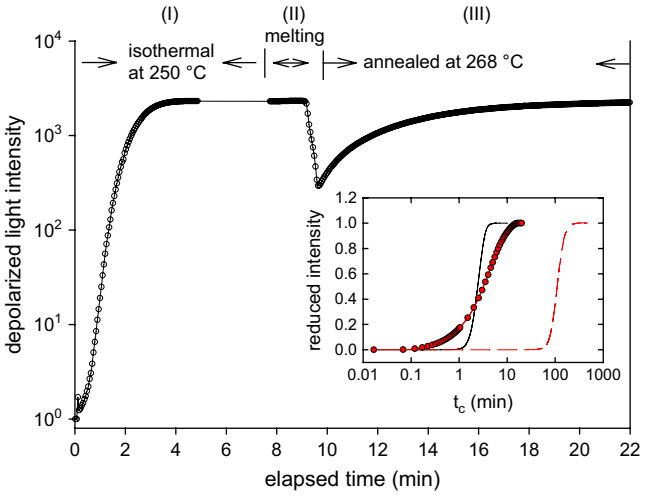

Fig. 7. Variation of depolarized light intensity during isothermal crystallization at 250 °C for 7.5 min first (*Stage I*), then heating at a rate of 10 °C/min to 268 °C (*Stage II*), and holding for re-crystallization up to 22 min (*Stage III*). The inset shows the crystallization evolution of sPS measured by PLM; the filled circles are results for the sPS re-crystallization at 268 °C, and the solid line and dashed line are results for sPS isothermally crystallized at 250 and 268 °C, respectively.

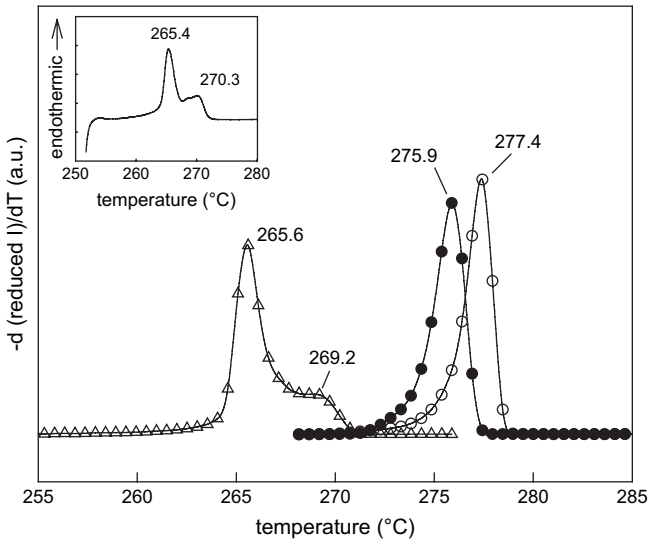

Fig. 8. Determination of melting temperature by PLM after various thermal treatments; (△): after isothermal crystallization at 250 °C; (○): after isothermal crystallization at 268 °C, and (●): after re-crystallization at 268 °C. The inset is the DSC melting curve of samples isothermally crystallized at 250 °C. The heating rate is 10 °C/min.

monitoring the re-crystallization evolution, which is referred to as *Stage III* (9.3–22 min). It is of interest to note that majority of the crystals developed at 250 °C are melted away during the *Stage II*, but crystal recovery during annealing at 268 °C is tremendously fast; within 10 min, the re-crystallization reaches its full capacity. The reduced intensity, expressed by $[I(t_c) - I_o]/[I_\infty - I_o]$ where I_o, I_∞, and $I(t_c)$ are the transmitted intensities measured at the initiation, saturation, and crystallization time of t_c, respectively, was used to represent the relative crystallinity developed during the phase transformation. The inset of Fig. 7 shows the evolution of relative crystallinity in *Stage I* (solid line) as well as that in *Stage III* (filled circles). Also given in the inset is the crystallinity evolution of the sPS samples that were melt-crystallized isothermally at 268 °C (dashed line) for comparison. According to the inset, the induction time required for the isothermal crystallization at 268 °C (~90 min) is significantly higher than that at 250 °C (~1 min). For the annealing process at 268 °C (*Stage III*), however, the induction time is significantly reduced to 0.2 min, indicating that the surviving crystals after partial crystal melting serve as the nuclei for the re-crystallization to readily take place. Based on the Avrami equation, the exponent and rate constant are derived to be 3.4 and 7.69×10^{-2} min^{-1}, respectively, for 250 °C isothermal crystallization, and 3.4 and 3.18×10^{-7} min^{-1}, respectively, for 268 °C isothermal crystallization. For the 268 °C annealing process (*Stage III*), on the other hand, the rate constant is ca. 1.89×10^{-1} min^{-1} and the Avrami exponent is changed to 1.2, which is in accord with the DSC results (Tables 2 and 3). This also suggests the one-dimensional crystal growth during the re-crystallization process.

After annealing at 268 °C (*Stage III*), the re-crystallized sample was heated under PLM to observe the morphological variation during melting, and the melting behavior is shown in Fig. 8 (solid circles) where the temperature derivative of the reduced intensity is plotted as a function of temperature. Thus, melting is in progress if the calculated $-dI/dT$ curve is above the baseline determined from the low and high-temperature extremes where no variation of light intensity should occur ($dI/dT \sim 0$). Fig. 8 also shows the melting curves determined in this manner for the samples isothermally crystallized at 250 °C (open triangles) and 268 °C (open circles), respectively. A single melting peak at 277.4 °C is observed for samples crystallized at 268 °C, whereas two melting peak temperatures are apparently discernible at 265.6 and 269.2 °C after crystallization at 250 °C, which is consistent with the DSC results (265.4 and 270.3 °C) as displayed in the inset. It should be noted that the high-temperature endotherm is relatively smaller than that for the quenched sample heating from the room temperature (Fig. 2). In addition to the direct observation of morphological changes, therefore, measurements of transmitted light intensity under PLM also provide a feasible route for determining the melting temperature. After complete crystallization at 250 °C, subsequent annealing of the samples at 268 °C for a short time (12.7 min) produces thickened lamellae, which are melted at a higher temperature of 275.9 °C. This is comparable to that of the samples isothermally crystallized at 268 °C for a long time (~340 min).

3.5. Morphological variations as revealed by SAXS and TEM

The code of *sPS-C* was referred to the sample which has been melt-crystallized at 250 °C for 2 h, followed by quenching to room temperature. As shown in Fig. 2, the DSC heating traces of the *sPS-C* showed two melting peaks at 264.1 and

Table 4
Morphological parameters of sPS samples experienced various thermal treatments

Code	ϕ^{WAXD}	$Q \times 10^2$	L_B (nm)	T_m (°C)	l_c (nm)
sPS-C	0.384	2.80	17.6	264.1/270.8	5.0/6.7
sPS-1	0.309	1.58	18.3	271.9	7.1
sPS-30	0.400	2.15	19.9	274.6	8.3

sPS-C is the sample melt-crystallized at 250 °C for 2 h prior to liquid nitrogen quenching; *sPS-1* and *sPS-30* are samples prepared by heating the *sPS-C* at a rate of 10 °C/min to 268 °C for annealing for 1 and 30 min, respectively, prior to liquid nitrogen quenching.

270.8 °C, respectively. To reveal the morphology variation occurring during partial melting, the originally crystallized *sPS-C* was heated at a rate of 10 °C/min to 268 °C and held isothermally for 1 min (sample *sPS-1*) and 30 min (sample *sPS-30*), respectively, prior to being quenched into liquid nitrogen. It is noted that the selected temperature of 268 °C is sufficiently high to completely melt the lamellae associated with the first melting peak (Fig. 8) for further investigating the un-melted lamellae together with the thickened ones due to re-crystallization. The WAXD intensity profiles of these samples show the preservation of β′-form modification, and the determined ϕ^{WAXD} is tabulated in Table 4. Accordingly, Figs. 9 and 10 show the SAXS intensity profiles and TEM images of the corresponding samples, respectively, for revealing the morphological variation of the lamellae developed. The plots of Lorentz-corrected intensities versus scattering vector, q, of the samples measured at room temperature are shown in Fig. 9. In addition to the presence of scattering peak, strong scattering at the lower q regions is evidently observed as shown in Fig. 9a. The Debye–Bueche model was applied to account for this peculiar scattering. A detailed discussion of this unique scattering has been provided in a previous article [27]. After subtraction of the zero-angle scattering intensity, I_o, the modified Iq^2–q plots are shown in Fig. 9b to reveal the contribution resulting exclusively from the lamellar morphology. Based on the Bragg's law, the position of the intensity maximum (q_m) was used to derive the long period L_B ($=2\pi/q_m$) [36]. The scattering invariant, Q, determined from the area under the Iq^2–q curve (Fig. 9b) represents the scattering power of the sample. Annealing of the *sPS-C* sample at 268 °C for 1 min, as shown in Table 4, results in the L_B increase from 17.6 to 18.3 nm and the reduction of ϕ^{WAXD} and Q due to the crystal melting [36]. It is intriguing to note that an extended annealing to 30 min gives rise to the gradual increase of the L_B and Q as well as ϕ^{WAXD}, indicating the additional contribution resulting from further re-crystallization. Also given in Table 4 is the lamellar thickness, l_c, determined from the measured melting temperature along with the Gibbs–Thomson equation using an equilibrium melting temperature of $T_m^o = 291$ °C and $\sigma_e/\Delta H_f^o = 0.12$ nm for the β-form sPS, where σ_e is the surface energy of the fold surface [37]. Typical lamellar morphologies are illustrated in Fig. 10 where the bright lines are associated with crystalline lamellae with which its thickness is given by the line width. Apparently, the *sPS-C* sample is filled with dense lamellae with a thickness of

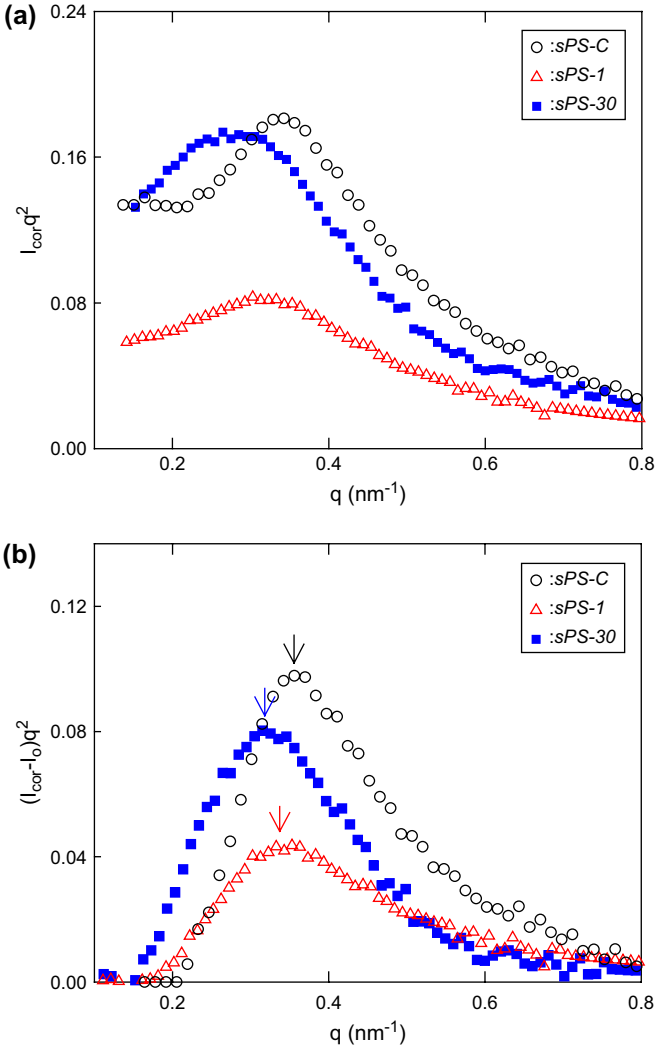

Fig. 9. Lorentz-corrected SAXS intensity plots of samples measured at 25 °C (a) without and (b) with subtraction of the intensity associated with the zero-angle scattering, I_o, determined from the Debye–Bueche model. *sPS-C* is the sample isothermally crystallized at 250 °C for 2 h and then rapidly cooled. Sample *sPS-1* is obtained by heating *sPS-C* at a rate of 10 °C/min to 268 °C, holding for re-crystallization for 1 min, and then quenching to liquid nitrogen. Sample *sPS-30* is obtained by heating *sPS-C* at a rate of 10 °C/min to 268 °C, holding for re-crystallization for 30 min, and then quenching to liquid nitrogen.

~7 nm. However, the annealed samples (*sPS-1 and sPS-30*) possess a lower population of lamellae with higher thicknesses (~10 nm), leading to a more vivid TEM observation. A higher TEM magnification for the *sPS-C* is displayed in Fig. 11. The typical regions (A, B, C, and D) are highlighted and are indicative of the existence of thin lamellae growing in-between two thick neighbors, which favors the lamellar insertion model [14,38].

3.6. A proposed mechanism for re-crystallization

Under e-beam radiation, the amorphous region will be selectively attacked first in comparison with the ordered crystalline region, and this is due to the presence of excess free

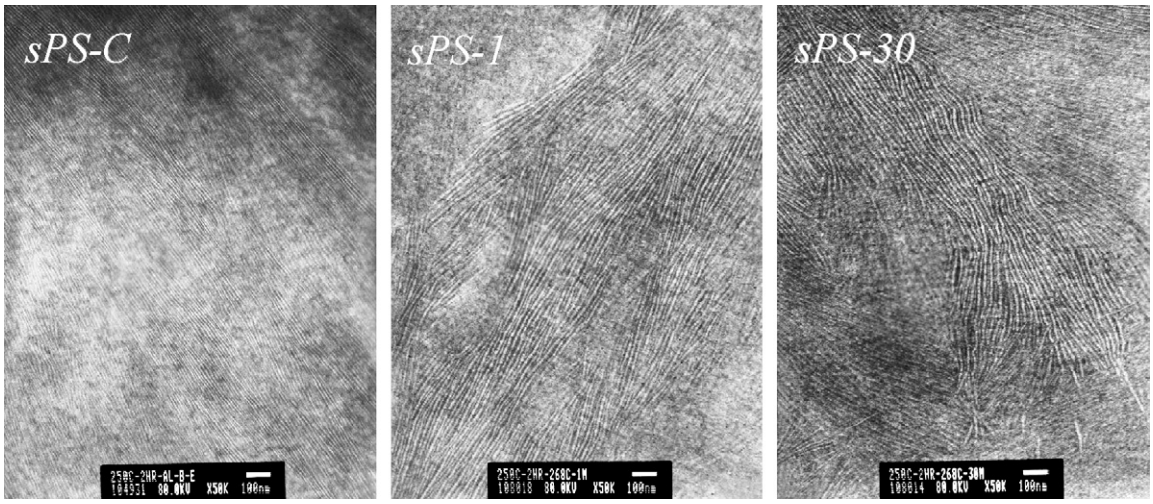

Fig. 10. TEM images of various sPS samples. The sample codes are the same as those given in Fig. 9. The scale bar is 100 nm.

volume. Lamellar crystals will eventually be affected for the samples subjected to excessive e-beam bombardment. Based on the dual lamellar stack model [13,15], separate stacks with the thin and thick sPS lamellae are developed after crystallization at 250 °C. The low- and high-temperature endotherms represent the melting of stacks filled with thin and thick lamellae, respectively. Apparently, the lamellar stacks with thicker crystal thickness possess a higher radiation resistance than those stacks with thinner crystals. If the dual lamellar stack model were applied for accounting the double melting of the β-form sPS, the suppression of the low-temperature endotherm would be more severe than the high-temperature one. On the basis of Fig. 2, however, the position and magnitude of the high melting peak were evidently decreased under a low-level radiation, and it eventually disappeared when a critical dose was imposed. Thus, our study's e-beam radiation results are against the dual lamellar stack model, but it lends support strongly for the re-crystallization model. Moreover, on the basis of the morphological evidence (Fig. 11), a combination of two events should be considered together to account for the double melting behavior of β′-form sPS [39], namely, (1) a broad distribution of lamellar thickness resulting from the lamellar insertion habit, and (2) melting, re-crystallization, and re-melting phenomena.

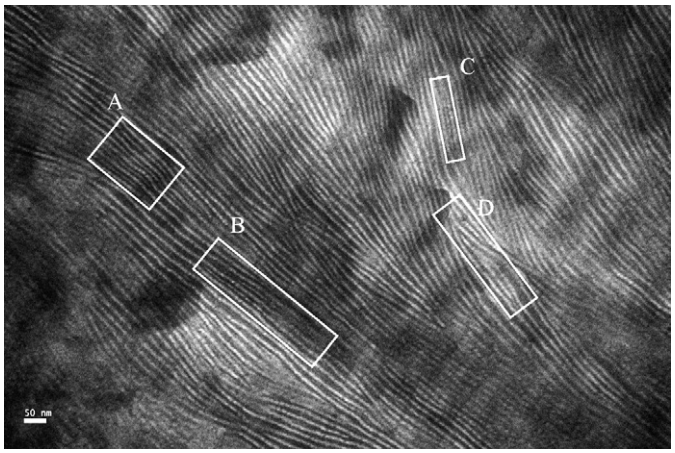

Fig. 11. TEM image of *sPS-C* samples with high magnification. Regions A, B and C show the existence of short and thin lamellae trapped in-between two long and thick lamellae. Region D shows the lamellar branching and isolated lamellae. The scale bar is 50 nm.

Due to the sheaf-like unidirectional growth of sPS lamellar stacks to fill out the space available [26], a broad distribution of lamellar thickness is not unexpected within sPS spherulites (or axilites). Through branching and fanning in the intermediate stages of sheaves, the main framework of the spherulites is constructed by the thicker lamellae; in the meantime, some inter-lamellar regions, if sufficiently wide, become available for the accommodation of a thinner lamella, as shown in Fig. 11. Indeed, the thin inserted lamellae with a short lateral dimension are readily observed and are widely distributed within the sPS spherulites. The inserted lamellar nuclei could be developed by the loose loop (or cilia) of polymer chains, which still remains within the melt region although the rest of the chain segments have been already crystallized into the neighboring lamella. Based on our TEM observations, the population of these inserted lamellae is gradually reduced with increasing T_c. Due to the rapid crystallization process at a high undercooling (low T_c), the spacing between two growing lamellae becomes more non-uniform, and more local regions suitable for the subsequent residence of the inserted lamellae are available. Being developed in an intervening and restricted space, the inserted lamella is less stable than its neighbors and will be the first to melt.

After an inserted lamella within the stacks disappears, the localized amorphous layer becomes larger. The following question then arises: will a new lamella form in this melted region? The formation of a new lamella in this localized melt pool is unlikely to take place since severe difficulties will be encountered in developing a thicker nucleus in such a limited time (Fig. 7) at a higher annealing temperature (268 °C). If it were to occur, on the other hand, the long period would be reduced, which is inconsistent with the SAXS results (Table 4). Then another crucial question arises: where do the thickened lamellae associate with the re-crystallization process?

Using a decoration method [40], Tosaka et al. [41] and Ho et al. [42] have shown that the polymer chains are irregularly folded even in the single lamellar crystals of sPS. The irregular folding habit of the sPS chains is further supported by a recent finding that the fold surface energy of the β′-form sPS lamellae is only slightly larger than its lateral surface energy [37]. The lack of uniform folding directions plausibly resulted from the presence of stacking faults [41,43], which influence the new polymer stem to attach onto the growth face. Essentially, the polymer chains on the lamellar surface are not tightly folded but act like ''floating segments'' [42] which possess sufficient mobility for conformation change induced by appropriate thermal treatments. In other words, short-term annealing at temperatures higher than T_{ml} tends to change the nature of the fold surface. After melting of the inserted lamella, the adjacent lamellae left behind are likely to be thickened by the tightening of loose folds or the withdrawal of cilia from the melt pool [44]. The population and ultimate thickness of the thickened lamellae are dependent on the heating rate as well as the annealing temperature (Tables 2 and 3). Thus, the high-temperature endotherm is associated with the melting of both the thickened lamellae and the lamellae initially present. A large amount of thickened lamellae essentially gives rise to the pronounced appearance of a high melting endotherm with a peak temperature of T_{mh} determined from the average thickness of the un-melted and thickened lamellae prior to the second melting.

Based on our above arguments, the high-temperature endotherm could be significantly suppressed if the population of the inserted lamellae were effectively reduced for not being able to trigger the re-crystallization process. To fulfill this condition, the blending of sPS with its atactic isomer (aPS) provided a feasible route. Since the interfibrillar segregation of the amorphous aPS was concluded in the sPS/aPS blends [27], the number of sPS lamellae in each stack was significantly reduced by excessive dilution. This is the same with the formation probability of the inserted lamellae. For the 10/90 blends melt-crystallized at 250 °C, stacks consisting of typical 4–7 lamellae were seen, and no inserted lamella was found under TEM observations [27]; the DSC results showed a single melting temperature at 265.0 °C which was identical with T_{ml} of the neat sPS (Fig. 8). Our model is also consistent with a previous finding by Chiu and Peng [22] that the re-crystallization extent of the aPS/sPS blends was primarily dependent on the crystallization rate of sPS regardless of the T_c and the molecular weight of aPS used. As a matter of fact, a higher crystallization rate of sPS generally produces a lamellar stack morphology with more inserted lamellae, which in turn enhances the re-crystallization behavior during the melting scan.

4. Conclusions

The objectives of this work were to explore the origin of the double melting behavior of β′-form sPS, which was often observed for the samples melt-crystallized at a low temperature. After extensive e-beam radiation, the high-temperature peak was gradually suppressed and eventually disappeared at a dose of 1.8 MGy. It was concluded that e-beam radiation gave rise to the formation of chemical cross-linking occurring effectively between sPS crystalline lamellae, the purpose of which is to prohibit the re-crystallization of the melting lamellae. This indicates the invalidity of the dual thickness model to account for the double melting behavior of sPS. After radiation with a dose up to 2.4 MGy, no significant change of the WAXD intensity profiles was observed, suggesting the safe preservation of the β-form crystals. Regardless of the heating rate and annealing temperature, re-crystallization during the partial melting followed the mechanism of one-dimensional crystal growth according to the corresponding Avrami exponent, as evidenced by the DSC and PLM results.

On the basis of morphological observations, the lamellar insertion model was also verified to accompany the re-crystallization model to account for the double melting behavior of sPS. In other words, the initial melting is associated with the melting of thin lamellae existing in a restricted space in-between two thick lamellae. After the short and thin lamellae are melted away, the inter-lamellar regions left behind are available for the un-melted neighbors to further increase their thickness through one-dimensional growth process. Thus, the position of the high melting endotherm is dependent on the average thickness of the un-melted lamellae as well as the thickened ones relevant with the re-crystallization process.

Acknowledgment

This work has been supported through a grant from the National Science Council of the Republic of China (NSC91-2216-E-006-031) and we are also grateful to Dr. F.S. Liao in China Steel Corporation (Taiwan) for the assistance of e-beam radiation experiments.

Appendix. Supplementary data

Supplementary data associated with this article can be found, in the online version, at doi:10.1016/j.polymer.2007.10.012.

References

[1] Holdsworth P, Turner-Jones A. Polymer 1971;12:195.
[2] Alfonso CC, Pedemonte E, Ponzetti L. Polymer 1979;20:104.
[3] Cheng SZD, Cao MY, Wunderlich B. Macromolecules 1986;19:1868.
[4] Bassett DC, Olley RH, Al Raheil IAM. Polymer 1988;29:1745.
[5] Lee Y, Porter RS, Lin JS. Macromolecules 1989;22:1756.
[6] Lattimer MP, Hobbs JK, Hill MJ, Barham PJ. Polymer 1992;33:3971.
[7] Liu T. Eur Polym J 2003;39:1311.
[8] Lovering EG, Wooden DC. J Polym Sci Polym Phys Ed 1969;7:1639.
[9] Samuel RJ. J Polym Sci Polym Phys Ed 1975;13:1417.
[10] Cebe P, Hong SD. Polymer 1986;27:1183.
[11] Jonas AM, Russell TP, Yoon DY. Macromolecules 1995;28:8491.
[12] Dawson PC, Blundell DJ. Polymer 1980;21:577.
[13] Verma RK, Hsiao BS. Trends in Polym Sci 1996;4:312.
[14] Strobl G. The physics of polymers. Berlin, Heidelberg: Springer-Verlag; 1996. p. 181.
[15] Verma R, Marand H, Hsiao B. Macromolecules 1996;29:7767.

[16] Guerra G, Vitagliano VM, De Rosa C, Petraccone V, Corradini P. Macromolecules 1990;23:1539.
[17] Cartier L, Okihara T, Lotz B. Macromolecules 1998;31:3303.
[18] Chatani Y, Shimane Y, Ijitsu T, Yukinari T. Polymer 1993;34:1625.
[19] Tosaka M, Tsuji M, Kohjiya S, Cartier L, Lotz B. Macromolecules 1999; 32:4905.
[20] Hong BK, Jo WH, Lee SC, Kim J. Polymer 1998;39:1793.
[21] Sun YS, Woo EM. Macromolecules 1999;32:7836.
[22] Chiu FC, Peng CG. Polymer 2002;43:4879.
[23] De Rosa C, De Ballesteros OR, Di Gennaro M, Auriemma F. Polymer 2003;44:1861.
[24] De Rosa C, Rapacciuolo M, Guerra G, Petraccone V, Corradini P. Polymer 1992;33:1423.
[25] Sun YS, Woo EM. J Polym Sci Polym Phys Ed 2000;38:3210.
[26] Wang C, Chen CC, Cheng YW, Liao WP, Wang ML. Polymer 2002;43: 5271.
[27] Wang C, Liao WP, Cheng YW, Lin TL. Polymer 2004;45:961.
[28] Inomata K, Liu LZ, Nose T, Chu B. Macromolecules 1999;32:1554.
[29] Takashika K, Oshima A, Kuramoto M, Seguchi T, Tabata Y. Radiat Phys Chem 1999;55:399.
[30] Birkinshaw C, Buggy M. J Appl Polym Sci 1990;41:1913.
[31] Nichol JM, O'Donnell JH, Rahman NP, Winzor DJ. J Polym Sci Polym Chem Ed 1977;15:2919.
[32] Paszlor JR, Landes BG, Karjala PJ. Thermochim Acta 1991;177:187.
[33] Gianotti G, Valvassori A. Polymer 1990;31:473.
[34] Kim HG, Robertson RE. J Polym Sci Polym Phys Ed 1998;36:133.
[35] Ding Z, Spruiell JE. J Polym Sci Polym Phys Ed 1996;34:2783.
[36] Due to the proximity in the densities of the lamellar and amorphous layers, a weak SAXS reflection of sPS samples was usually obtained at room temperature. To enhance the density contrast, high-temperature SAXS scattering [27] provided a means to obtain sufficient scattering intensity for the precise determination of morphological parameters, such as the lamellar thickness (l_c) and amorphous layer thickness (l_a), in addition to the long period, by further scattering intensity analyses using the correlation function method or interface distribution function approach. However, annealing at an elevated temperature, e.g. 150 °C, would further advance the crystallization of the *sPS-1* and *sPS-30* samples, giving a misleading result of l_c. Therefore, high-temperature SAXS was not conducted in this study, and the long periods at room temperature determined by the Bragg's law were displayed in Table 4.
[37] Wang C, Liao WP, Wang ML, Lin CC. Polymer 2004;45:973.
[38] Krüger K-N, Zachmann HG. Macromolecules 1993;26:5202.
[39] Melting of the re-crystallized lamellae cannot be simply used to account for the presence of high-temperature endotherm based on the following observations. Regardless of the heating rates ($R = 1-40$ °C/min) imposed on the β-form sPS samples melt-crystallized at 240 °C, two melting peaks were always detected during the heating scans. With increasing R, T_{ml} was increased but T_{mh} remained relatively unchanged, and their separation was gradually diminished (shown in Fig. 1, Supplementary data). Similar trend was also reported by Hong et al. [20] and De Rosa et al. [23]. In addition, the ratio of the endotherm heights (H_{mh}/H_{ml}) was gradually decreased with increasing R up to 10 °C/min, and leveled off at a higher R. These findings violate the characteristics of re-crystallization model, i.e. with increasing R, (1) T_{ml} will increase but T_{mh} should decrease, and (2) the height of low-temperature endotherm will increase but that of high-temperature endotherm will continuously decrease, giving a monotonic decreasing ratio of H_{mh}/H_{ml}.
[40] Wittmann JC, Lotz B. J Polym Sci Polym Phys Ed 1985;23:205.
[41] Tosaka M, Hamada N, Tsuji M, Kohjiya S, Ogawa T, Isoda S, et al. Macromolecules 1997;30:4132.
[42] Ho RM, Lin CP, Hseih PY, Chung TM. Macromolecules 2001;34:6727.
[43] Tosaka M, Hamada N, Tsuji M, Kohjiya S. Macromolecules 1997;30: 6592.
[44] Bassett DC, Patel D. Polymer 1994;35:1855.